Collaborative project*

Project acronym: SNM

Project full title: "**Single Nanometer Manufacturing for beyond CMOS devices**"

Grant agreement no: 318804

Deliverable: D2.5 ("Nanometer precise 3D patterns")

Name of the coordinating person: Prof. Dr. Ivo W. Rangelow, Email: ivo.rangelow@tu-ilmenau.de

List of participants:

Participant no.	Participant organisation name	Part. short name	Activity Type	Country
1 (Co)	Technische Universität Ilmenau	**TUIL**	HER	Germany
2	EV Group E. Thallner GmbH	**EVG**	IND; End-user	Austria
3	IMEC	**IMEC**	RES	Belgium
4	Mikrosistemi Ltd	**µS**	SME; End-User	Bulgaria
5	Universität Bayreuth	**UBT**	HER	Germany
6	Technische Universiteit Delft	**TUD**	HER	Netherlands
7	Spanish National Research Council	**CSIC**	RES	Spain
8	IBM Research GmbH	**IBM**	IND; End-user	Switzerland
9	École polytechnique fédérale de Lausanne	**EPFL**	HER	Switzerland
10	SwissLitho AG	**SL**	SME; End-User	Switzerland
11	Oxford Instruments Nanotechnology Tools Ltd	**OINT**	IND; End-user	UK
12	Imperial College London	**IMPERIAL**	HER	UK
13	The Open University	**OU**	HER	UK
14	Oxford Scientific Consultants Ltd	**OSC**	SME	UK
15	VSL Dutch Metrology Institute	**VSL**	IND	Netherlands
16	University of Liverpool	**ULIV**	HER	UK

SNM
Work Package 2
Deliverable: D2.5 ("Nanometer precise 3D patterns")

Lead beneficiary number	8	**Nature**	R	**Dissemination level**	PU
Estimated Person-months	30				

Person-months by partner for the Deliverable	IBM									
	21									

Estimated Delivery Date	M36: 1/2016	**Delivery Date**	31/1/2016
Author	• Colin Rawlings		
Reviewed by:	• WP2 Leader: Urs Duerig • WPG1 Leader: Armin Knoll • Coordinator: Ivo W. Rangelow		

Criteria and Achieved Results	**Criteria**	**Achieved result**
	Mitigate issues with thermal drift	Closed loop read scheme for controlling tip-sample separation with nanometer accuracy established using thermoresistive distance sensing.
	Demonstrate nanometer resolution in the z direction	Nanometer resolution demonstrated.
	Reliable fabrication of nanometer accurate 3D patterns	Demonstrated 1sigma errors below 1 nanometer for test patterns.

Description of the Deliverable	**Executive Summary** The last 50 years have seen steady improvement in the lithographic tools available to researchers and these tools have underpinned developments in a diverse range of fields in the physical sciences. Micro-fabrication conventionally proceeds layer-by-layer and so tool development has focused on the reproduction of 2D geometries. However, there are a good deal of applications in optics, nanofluidics and tribology for 3D profiles. Here we describe recent work to develop a means of fabricating precise 3D profiles using thermal scanning probe lithography. Following optimisation of our cantilever's stiffness and the implementation of a closed loop lithography process we demonstrate sub-nanometer 1σ errors in the depths of our written patterns. We show how this capability is applicable to the fabrication of artificial surface roughnesses for fundamental studies in the field of contact mechanics. ***Report attached***
Explanation of Differences between Estimation and Realisation	Much faster progress than originally anticipated was made. Remaining person months (6) according to the revised consortium agreement will be used for preparing a publication and for exploring novel applications.
Metrology comments	• 0.85nm 1sigma errors over a 6um x 6um pattern • Calibration was performed using a z piezo whose extension was measured using an optical interferometer

Fabrication of nanometer accurate 3D Profiles using thermal Scanning Probe Lithography

Abstract

The last 50 years have seen steady improvement in the lithographic tools available to researchers and these tools have underpinned developments in a diverse range of fields in the physical sciences. Micro-fabrication conventionally proceeds layer-by-layer and so tool development has focused on the reproduction of 2D geometries. However, there are a good deal of applications in optics, nanofluidics and tribology for 3D profiles. Here we describe recent work to develop a means of fabricating precise 3D profiles using thermal scanning probe lithography. Following optimisation of our cantilevers and the implementation of a closed loop lithography process we demonstrate sub-nanometer 1σ errors in the depths of our written patterns. We show how this capability is applicable to the fabrication of artificial surface roughnesses for fundamental studies in the field of contact mechanics.

Introduction

The semiconductor industry has contributed greatly to fundamental understanding of materials at the nanoscale through its development of nanofabrication techniques. Conventional semiconductor fabrication proceeds layer-by-layer and the lithography techniques which the industry developed are adapted to this paradigm. However, these approaches impose limitations on the geometry of the final nanostructures, which hamper investigation of many

*To whom correspondence should be addressed

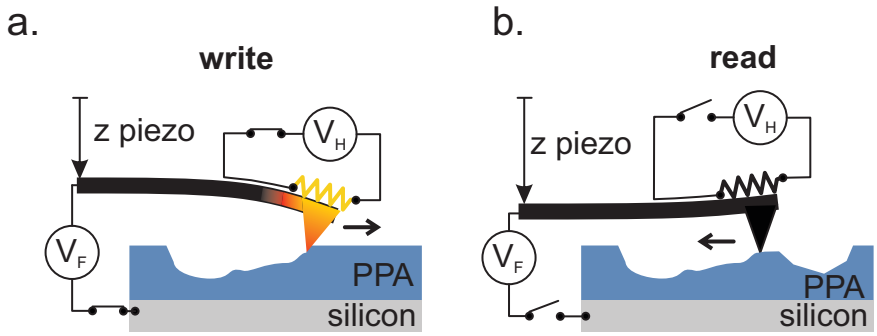

Figure 1: Closed loop lithography scheme used during 3D patterning. (a) Write mode: a voltage V_H is applied to the resistor located at the base of cantilever's tip. At each write pixel location a voltage pulse V_F is applied to the substrate to pull the tip into contact. (b) Read mode: the heater and substrate voltage are switched off and the z piezo is extended to bring the tip into contact with the surface. The written topography is read back and analysed. If necessary the patterning parameters for the next write line can then be adjusted.

fundamental phenomena. For example in optics edge effects associated with such geometries lead to scattering and limit the lifetime of photons in a cavity.[1] Conversely novel fabrication techniques,[2] which are not limited by this paradigm have yielded exciting developments in the field of meta-materials[3] and optics.[4]

Here we report on developments in the implementation of a nanometer precise technique for the fabrication of three dimensional surfaces using scanning probes. In this scheme a heated tip is used to locally remove a resist down to a carefully controlled depth[5,6] (see figure 1a). This technique has been shown to be capable of throughputs competitive with the current state of the art in maskless nanofabrication, Gaussian Electron Beam Lithography (EBL).[7] In addition it has been shown to be capable of sub-20 nm resolution and nanometer precise overlay.[8–10]

In this paper we demonstrate the implementation of sub nanometer patterning depth control using thermal scanning probes. This degree of control has been achieved firstly by optimising the stiffness of our homemade cantilevers. Secondly we have developed a model that allows for the accurate prediction of the patterning depth from the target depth via a pair of state parameters. These parameters are estimated using a static calibration procedure and then refined during patterning using the Kalman Filter formalism. We begin by outlining

the simple theory underpinning our system and then present results demonstrating our sub-nanometer control of the patterning process. We close by demonstrating that our patterning capability could be used to construct surfaces with a specific surface roughness. Such surfaces could be valuable tools in fundamental investigations of contact mechanics and cell adhesion.

Static Calibration

The electrostatic force between the cantilever and the surface may be obtained from the electrostatic potential distribution via the Maxwell stress tensor. At equilibrium this electrostatic force is balanced by internal stresses within the cantilever developed as it bends towards the surface. For the complex geometry of our cantilever an exact solution of these equations is only possible numerically. Fortunately our cantilever has in plane dimensions of several 10's of microns and a tip length of less than $1\,\mu$m. As such it may be anticipated that the deflection of the tip can be well modelled as a voltage supply V_F connected to a parallel plate capacitor C whose upper electrode is constrained by a spring of stiffness k (see figure 2a). The equilibrium deflection can be obtained from the energy of such a system: $-\frac{1}{2}C(d)V_F^2 + \frac{1}{2}kd^2$ where d is the electrode separation (see figure 2a, $d = l_{eff} + z_{ts}$). Specifically z_{ts} is obtained in terms of the system's effective parameters from the real root $x = (z_{ts0} - z_{ts})/(l_{eff} + z_{ts0})$ of the equation:

$$x: \quad x^3 - 2x^2 + x = V_F^2 \frac{\epsilon A_{eff}}{2k(z_{ts0} + l_{eff})^3}, \quad \Im(x) = 0 \tag{1}$$

where A_{eff} is the effective area of the parallel plate capacitor, ϵ is the dielectric permittivity and l_{eff} is the effective length of the cantilever tip. z_{ts0} is the tip-sample separation in the absence of an applied voltage. These equations are only valid for the cantilever in equilibrium when the tip-sample force is negligible.

The pull-in voltage required to pull the tip onto the surface therefore depends quadrati-

cally on the intial ($V_F = 0$) tip-sample separation z_{ts0} as:

$$z_{ts0} = \frac{\epsilon A_{eff}}{2kl_{eff}^2} V^2 \tag{2}$$

During patterning the substrate voltage is switched by means of a solid state relay on a timescale that is short in comparison with the mechanical time constants for the cantilever system. As such dynamic effects cannot be neglected. Representative values for the static and dynamic behaviour of our optimised, stiffer (cf. $k = 0.065\,\mathrm{Nm}^{-1}$ in ref. [5]) cantilevers are:

$$k = 0.3\,\mathrm{Nm}^{-1}, \quad f_R = 135\,\mathrm{kHz}, \quad Q = 33 \tag{3}$$

The stiffness[a] represents a comprimise between ensuring the cantilever dynamics dominate the tip-sample interaction and minimising tip-sample contact forces during read-back. The Q factor represents the relative energy loss per cycle. Ignoring the non-linear nature of electrostatic force the peak dynamic deflection for a given V_F will be a factor of $2(1-1/2Q) \simeq 2$ times greater than the static deflection. This peak deflection (see figure 2d) is obtained roughly $4\,\mu$s after the switch on of V_F . In our system the voltage pulse is therefore applied for $5\,\mu$s so that the cantilever executes a single swing for each write pixel.

[a]The stiffness was obtained from a finite element simulation, the cantilever thickness was measured using a scanning electron microscope. The material properties were taken from.[11]

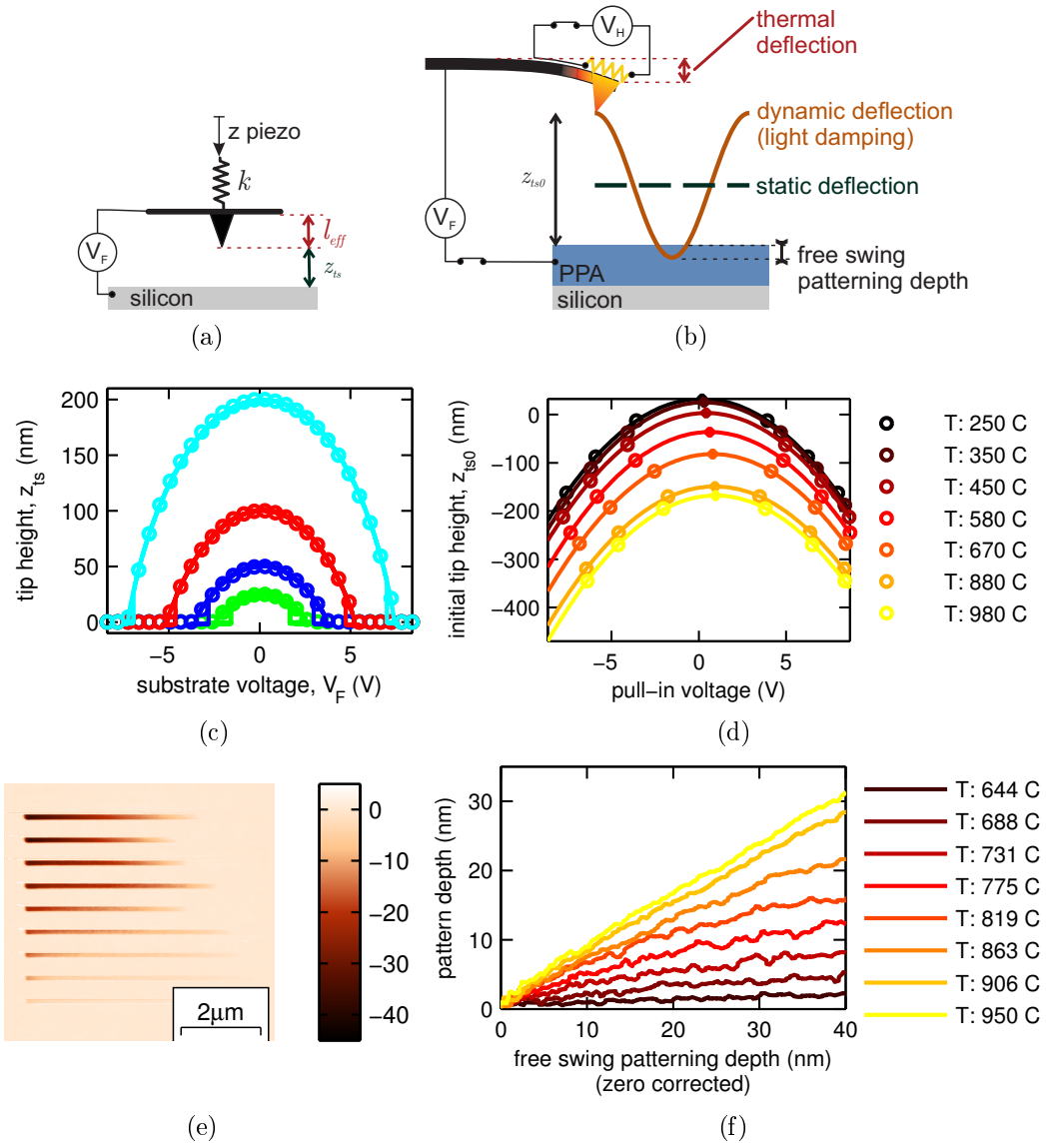

Figure 2: Experimental measurement of cantilever dynamics. (a) Effective capacitor-spring system. (b) The static and dynamic deflections for the lightly damped cantilever system (Q$\simeq$ 33). (c) The cantilever's tip height above the surface as a function of substrate voltage V_F for $z_{ts0} = 25\,\text{nm}$, $50\,\text{nm}$, $100\,\text{nm}$ and $200\,\text{nm}$. The experimental measurement is shown by the line, the circles are a least squares fit of (eq (1)). (d) Substrate voltage required to pull the tip onto a silicon surface from a given tip-sample separation z_{ts0} for different writer temperatures. (e) tSPL topography image following the patterning of a series of 10 pixel (114 nm) wide lines each written at a different heater temperature in a 110 nm thick PPA resist film. V_F has been steadily reduced moving from write to left. (f) The measured patterning depth for the center of each written line as a function of the free swing patterning depth. A z offset has been applied so that the curves pass through the origin since the calibration is not exact.

Figure 2b shows the measured tip height as a function of substrate voltage V_F for a silicon substrate. This measurement is possible because the cantilevers have integrated thermoresistive distance sensors[12] which, in contrast to a conventional optical lever setup, can measure absolute separation. This sensor is calibrated by approaching the cantilever towards the surface using the z piezo and recording the signal. As such we rely on the calibration of the piezo which was performed by the manufacturer using an optical interferometer. Results are shown by the solid lines for four lift heights z_{ts0} at $V_F = 0$. The circles shown the results of a simultaneous least squares fit of equation (1) to the four experimental curves. The fitted effective values were:

$$l_{eff} = 1.04\,\mu\text{m}, \quad \frac{\epsilon A}{k} = 3.9 \times 10^{-21}\,\text{Vm} \qquad \Rightarrow \sqrt{A_{eff}} = 11.5\,\mu\text{m}$$

These effective values are in reasonable agreement with the actual in-plane area and tip length ($\simeq 700\,\text{nm}$) of the cantilever. The fitted values are in excellent agreement with the experimental values across the full range of tip-sample separations. Perhaps more importantly the close agreement between the fitted and measured cantilever deflections suggest that equation (1) can be used to accurately describe the cantilever's static deflection.

Figure 2c shows results obtained with the cantilever operated in write mode. In write mode the cantilever may be heated via the resistive element located at the base of the tip. This heater can also be used to measure tip-sample separation and hence detect when the substrate voltage V_F reaches a level sufficient to pull the tip onto the surface. This voltage is measured for a range of lift heights and heater voltages. For a given heater voltage the lift height to pull in voltage defines a parabola (equation (2)). The heater calibration was performed using an I-V curve to detect the maximum in heater resistance. This occurs at a well defined temperature which depends on dopant density. Away from this maximum we assume the heater temperature depends linearly on dissipated power. Detailed finite element simulations as well as Raman measurements, which will be presented elsewhere, have shown

that the error in the calculated temperature rise using this assumption is around 10%.

Fitting a parabola through the sets of measurements performed at a fixed heater temperature reveals an important non-ideality in our system. The maximum of the parabola is not at the origin and instead exhibits a temperature dependence. The zero position for the y axis was identified by performing an approach curve using the z piezo and recording the position at which contact with the surface was detected. From examination of figure 2c it can be seen that heating the cantilever results in a thermal deformation which bends the tip towards the surface. Evidently the fabrication process for our cantilever's leads to an assymetry which in turn results in a thermal bimorph effect.

The thermal deformation must be accounted for when calculating the required write voltage. However, the deformation is still small in comparison to the in-plane length scale of the cantilever and as such we can treat it as an offset to the z position in our calculations. An additional effect is a shift of the maximum towards positive voltages. This results from the positive voltage V_H applied to the cantilever's write resistor to achieve the required temperature. This effect must also be included when calculating the write voltages.

Figure 2e shows a tSPL topography image recorded while writing 10 pixel wide lines into a PPA film, Each line has been written at a different temperature and the voltage V_F was varied along the line. The tip-sample separation used for writing was 300 nm. For each combination of V_F and V_H the free swing depth below the surface was calculated from equation (1). A z offset has been applied so that the curves pass through the origin since the static calibration is not exact.

It can be seen from figure 2f that at higher temperatures the patterning depth increases and indeed the patterning depth exhibits a bi-linear dependence on the free swing depth. At lower depths the slope is close to one while above a critical depth the slope drops. The roughness of the line is also greater at lower temperatures. This is possibly because the tip-sample interaction is less well defined than in the limiting single swing case relevant to the slope $\simeq 1$ regime. The statistical nature of the polymer decomposition at low temperatures

may also play a role.

Overall, our simple model (equation (1)) provides an accurate description of the cantilever dynamics. Furthermore at high temperatures ($\simeq 900°$C) the system exhibits behaviour which is both highly reproducible and linear. Thus the model and calibration scheme has reduced what was *a priori* a very complex dependence of patterning depth on the control voltages V_H and V_F (see figure 1) to a simple linear model. The static calibration identifies the zero position of the curves in figure 2f to an accuracy of typically ± 20 nm and for high temperatures predicts the slope to an accuracy of around 20%. To write a pattern with sub-nanometer error the value of these two parameters must be refined for the temperature and height selected for patterning. This refinement process should take place continuously to account for any drift in the parameters during writing. Our implementation of such a process will be discussed in the next section.

Control of the patterning process

Following the static calibration there is a residual uncertainty in the position and slope of the line relating free swing patterning depth to the observed patterning depth. As such we can relate the written depths z_w to the free swing depths z_{free} via the parameters z_{offs} and m:

$$z_w = z_{offs} + m z_{free} \tag{4}$$

Immediately following the calibration our best estimate of these parameters is $z_{offs} = 0$ and $m = 1$. During patterning we inspect the written pattern and use the information gained to select more accurate values for z_{offs} and m for the given write conditions.

To perform this process we employ the Kalman algorithm. As such the state of the system considered by the Kalman filter is parameterised by (z_{offs}, m). The Kalman algorithm is responsible for determining the optimal correction to the current estimate of the state given a measurement and that measurement's uncertainty. During scanning our computer

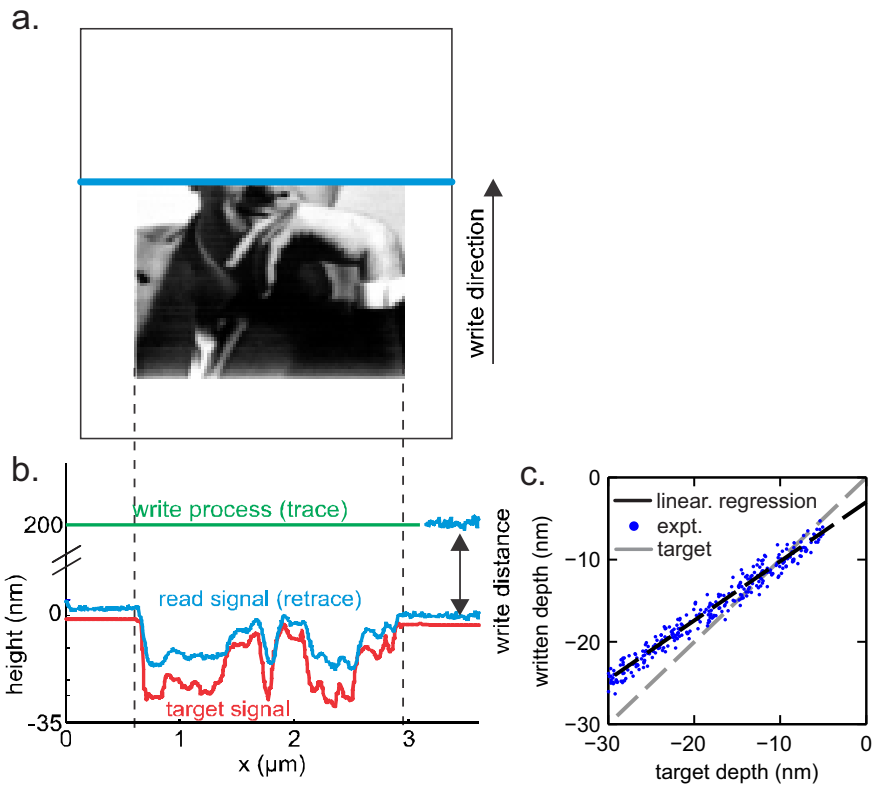

Figure 3: Control scheme employed during patterning to compensate for errors in the static calibration. (a) The 3D profile is written using a raster scan. (b) Each written line is read back as the cantilever moves in the retrace direction (see figure 1). (c) For each pixel the written and target depths are compared. A linear regression is used to extract the slope and offset parameters from this data. The Kalman filter is used to update the slope and offset state variables based on this measurement.

continuously performs this measurement by analysing batches of a fixed number (typically 100 points) of written and target depths (see figure 3b). The measurement and its associated uncertainty is obtained from a linear regression of the written and target depths for this set of points (see figure 3c). After the regression the computer implements the Kalman algorithm to calculate the optimal Δm and Δz_{offs} given this measurement. The next line is then written using the updated state $(z_{offs} + \Delta z_{offs}, m + \Delta m)$ to calculate the force voltage V_F for each write pixel. Once sufficient points have been patterned with this updated state the analysis process is repeated to identify a further correction to the state.

We supplement the Kalman scheme with several "common sense" checks on the input data to the linear regression. For example points where the written depth is zero cannot be

used and if all observed written depths are zero we simply increase z_{offs} by a pre-defined step. Likewise if all target depths for the given sample are the same then we only apply the Kalman filter to z_{offs} and remove m from consideration until patterning data for distinct depth levels becomes available.

Stabilisation of the write height is an important additional consideration for achieving precise depth control. Any errors in the tip sample separation z_{ts0} will appear directly in the pattern. We implement sub nanometer control of z_{ts0} using the following procedures. Firstly after loading a sample we use the thermoresistive distance sensor to measure the sample tilt, which is typically on the order of $1\,\mathrm{nm}/\,\mu\mathrm{m}$. To measure the tilt the tip is retracted 100 nm from the sample and the sample is then scanned in first the x and then the y direction. The change in tip-sample separation during this motion is recorded and the tilt is calculated from this signal. This tilt is then used when calculating the scan trajectory. During scanning the extension of the z piezo changes as the tip moves between the read and write heights (see fig 1). To ensure this motion is accurate we employ a feed forward scheme.[7] We have observed that the z position of our tSPL system drifts by several nanometers during the patterning process, possibly because of heating of the piezos. To compensate for this drift we measure the change in reader signal during the retract and approach to the surface occuring when switching between the read and write heights. From these signals the absolute height of the system can be determined and the position drift accounted for.

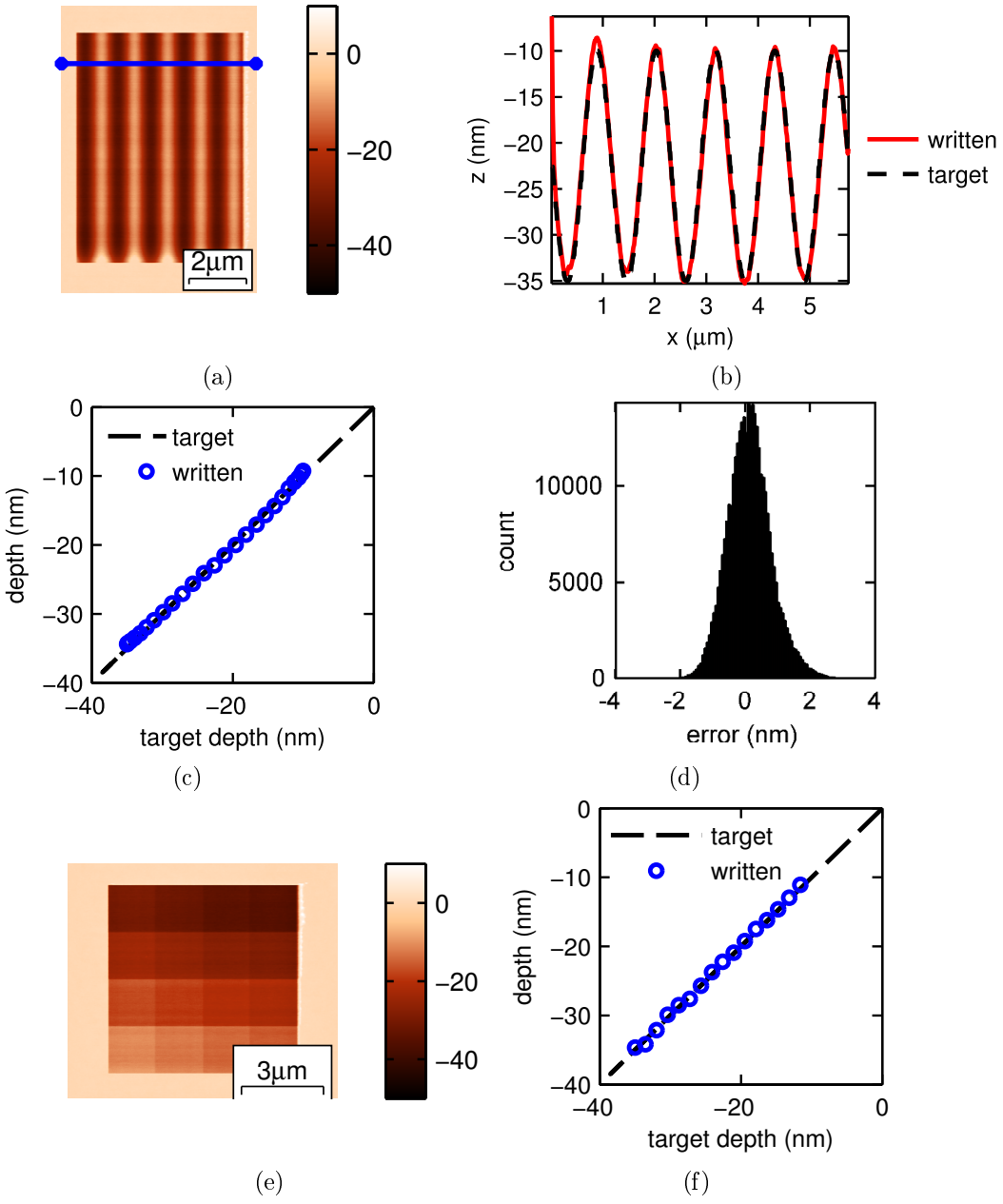

Figure 4: 3D patterns written into a 110 nm thick PPA film to quantify the accuracy of the closed loop lithography process. Write pixel size was 11.4 nm, read pixel size was 5.7 nm. One write pixel was written every 15 μs. (a) tSPL topography image of a sine wave pattern written between depths of 10 nm and 35 nm. (b) Comparison between the written and target depth along the blue cross section of (a). (c) Written vs target depth for each depth level in the upper 75% of the pattern in (a). (d) Histogram for the errors in write depth for the pattern in (a). (e) tSPL topography image of a 4×4 chequerboard pattern. (f) Written vs target depth for each depth level in (c).

Results

Test Patterns

Figure 4 shows the result of using the closed loop lithography process to write a pair of test patterns. The result of writing a sine wave in a 110 nm thick film between depths of 10 nm and 35 nm is shown in figure 4a. The variation visible in the lower 10% of the pattern occured as the feedback loop corrected for errors in the static calibration. A comparison between the written and target depths along the blue cross section shown in figure 4a is shown in figure 4b. The average written depth for the upper 75% of the pattern for each target depth is shown in figure 4c. The pixels in the first (bottom) 25% of the image were not included in the analysis since the feedback loop was still correcting for the errors in the static calibration. The error distribution for all depth levels in the final 75% of the pattern is shown in figure 4d. Figure 4e shows the result of writing 16 tiles each at a fixed target depth. The corresponding relationship between written and target depth is shown in figure 4f. The 1σ error for the two patterns was:

$$\text{Sine wave}: \quad 1\sigma = 0.85\,\text{nm}, \quad \text{Chequerboard}: \quad 1\sigma = 0.69\,\text{nm}$$

These roughnesses compare favourably with the intrinsic roughnes of a spin cast polymer film of $\simeq 0.5\,\text{nm}$.[13]

Artificial surface roughness

The interactions between rough surfaces govern a variety of phenomena from the transport of heat to the friction developed between sliding surfaces. Such interactions have great engineering significance and Nature is particularly expert at optimising surfaces to achieve a particular function.[14] In general the macroscopic property of the interface will depend on the material's response to applied stress, the interactions present between the interfaces

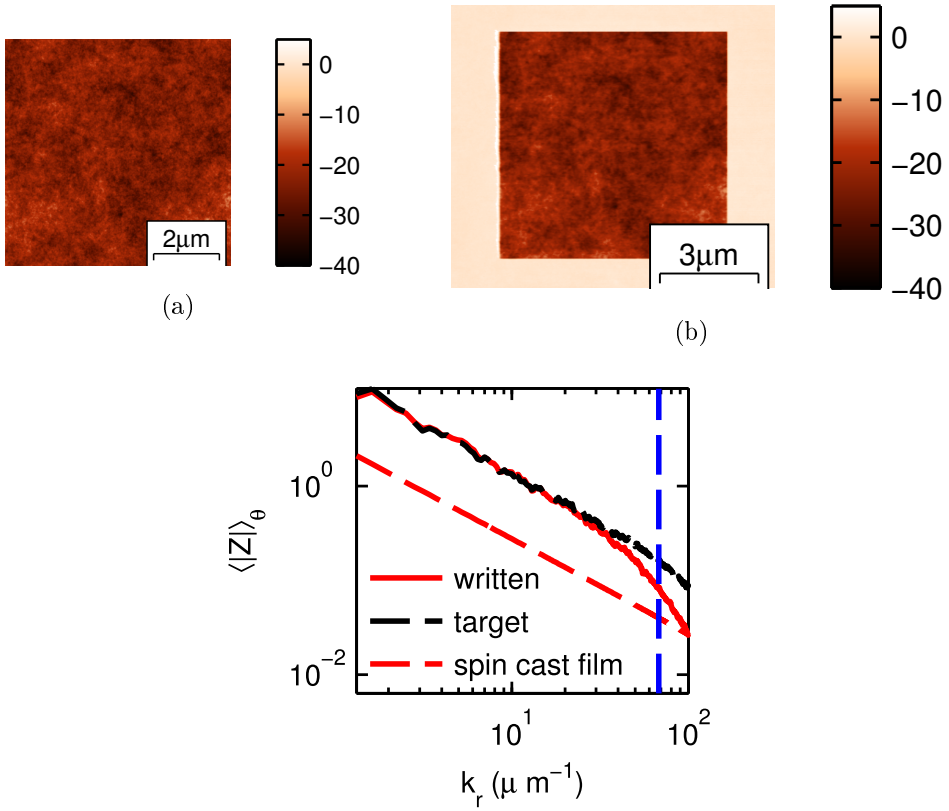

Figure 5: Fabrication of an artificial surface roughness using tSPL. (a) Target topography. A random number generator was used to construct an image whose frequency content $|Z(k_x, k_y)| = |\mathcal{F}\{z(x, y)\}|$ was proportional to $1/|k|$. The target depth range was between -10 nm and -35 nm. (b) The result of writing the image of (a). (c) Comparison between the frequency content of the target and written images. The signal has been averaged with respect to the direction of the wave vector (see equation (5)). The blue dashed line shows the wavenumber at which the written amplitude falls to half of its target value. The red dashed line shows the theoretical frequency content of a spin cast film having an RMS surface roughness of 0.5 nm.

and the geometry of the interface itself. Starting with Hertz great progress has been made in establishing the relationship between these interface and material properties.[15,16] The fabrication technique presented here can simplify the experimental investigation of recently developed theories[17] in which the frequency content of the surface features prominently. Using tSPL it is possible to define an artificial surface "roughness" spanning a length scale from several 10's of nanometers up to several 10's of micrometers. With these surfaces it would be possible to test experimentally the effect of the frequency content of the surface topography *ceteris paribus* as well as engineer favourable roughnesses for the support of cells.

Figure 5a shows a simulated topography of such an artificial surface roughness. The amplitude of the frequency components from which this image is formed exhibits a power law dependence on wave number, $|Z| \propto 1/|k|$. This frequency content arises naturally at the interface between liquids and gases[18] and is "frozen" into the surface of a polymer film during the spin casting process as the solvent leaves the film. The maximium and minimium depths present in the topography are 10 nm and 35 nm respectively. Figure 5b shows the tSPL topography image taken after writing this pattern into the 110 nm thick PPA film. The frequency content of the target and written image is shown in figure 5c. The frequency content has been averaged with respect to the direction of the wave vector:

$$\langle |Z| \rangle_\theta = \tfrac{1}{2\pi} \int_0^{2\pi} |Z(k_r \cos\theta, k_r \sin\theta)| \; d\theta \tag{5}$$

At low frequencies the amplitude of the written frequency component is in good agreement with the target amplitude. However, at higher frequencies the amplitude of the written component drops due to the finite size of the probe used to fabricate the pattern. The written amplitude falls to half the target amplitude for a half wavelenth of:

$$\lambda_c/2 = 46\,\mathrm{nm}$$

Recently we have demonstrated[8] that tSPL can be used to fabricate sub 20 nm features in comparison to this dimension and our observed value for λ_c is rather large. However, as can be observed in figure 2f, high tip temperatures are required for reliable patterning and as a consequence we see best 3D performance when working with blunter tips that offer a lower thermal resistance.

The theoretical frequency content of a spin cast film having a representative RMS surface roughness of 0.5 nm[13] is also shown in figure 5c. The low frequency cutoff k_{min} for this distribution was taken to be[19] $k_{min} = (A/2\pi\gamma t^4)^{0.5} = 0.02\,\mu\mathrm{m}^{-1}$ where A is the Hamaker constant, t is the film thickness and $\gamma = 0.03\,\mathrm{J/m}^2$ is the surface tension. It can be seen that

for the writing depths (10 nm to 35 nm) chosen here the written roughness has a significantly greater amplitude than the intrinsic roughness of the film (0.5 nm RMS). This could be of use during experimental investigations involving these structures. For elastic materials it can be shown that the interaction between a pair of rough surfaces having topographies $z_1(x)$ and $z_2(x)$ respectively is identical to the interaction between a perfectly flat surface and a surface having the topography $z_1 + z_2$. If an artificial roughness z_1 is fabricated for which $z_1 \gg z_2$ then the interaction becomes insensitive to z_2 reducing the complexity of the experimental system. If required a pattern transfer scheme could be employed[5,8] to amplify the height of the written pattern further or transfer it to a harder material.

Conclusions

The ability to precisely fabricate 3D profiles could help resolve interesting questions in fields ranging from optics to tribology. tSPL is a technique for producing such profiles which offers rapid turnaround and precise control. Despite the complexity of our cantilever geometry and the equations governing our tSPL system the dynamical behaviour of our cantilever can be accurately described by a single simple equation. We have shown that if the cantilever is operated at temperatures exceeding 900°C the patterning depth is repeatable and linearly related to the depth predicted by our calibration of the system. As a result it has been possible to achieve sub-nanometer control of the patterning depth through the implementation of a feedback scheme based on the Kalman filter formalism. Finally we have demonstrated experimentally that our system is suitable for the fabrication of artificial surface roughness

References

(1) Ding, F.; Stöferle, T.; Mai, L.; Knoll, A.; Mahrt, R. F. *Phys. Rev. B* **2013**, *87*, 161116.

(2) Fischer, J.; Wegener, M. *Laser & Photonics Reviews* **2013**, *7*, 22–44.

(3) Bückmann, T.; Thiel, M.; Kadic, M.; Schittny, R.; Wegner, M. *Nat. Commun.* **2014**, *5*, 4130.

(4) Schell, A. W.; Neumer, T.; Shi, Q.; Kaschke, J.; Fischer, J.; Wegener, M.; Benson, O. *Applied Physics Letters* **2014**, *105*.

(5) Knoll, A. W.; Pires, D.; Coulembier, O.; Dubois, P.; Hedrick, J. L.; Frommer, J.; Duerig, U. *Adv. Mater.* **2010**, *22*, 3361–3365.

(6) Pires, D.; Hedrick, J. L.; De Silva, A.; Frommer, J.; Gotsmann, B.; Wolf, H.; Despont, M.; Duerig, U.; Knoll, A. W. *Science* **2010**, *328*, 732–735.

(7) Paul, P. C.; Knoll, A. W.; Holzner, F.; Despont, M.; Duerig, U. *Nanotechnology* **2011**, *22*, 275306.

(8) Wolf, H.; Rawlings, C.; Mensch, P.; Hedrick, J. L.; Coady, D. J.; Duerig, U.; Knoll, A. *J. Vac. Sci. Technol., B* **2015**, *33*, 02B102.

(9) Rawlings, C.; Duerig, U.; Hedrick, J.; Coady, D.; Knoll, A. *IEEE Trans. Nanotechnol.* **2014**, *13*, 1204–1212.

(10) Rawlings, C.; Wolf, H.; Hedrick, J. L.; Coady, D. J.; Duerig, U.; Knoll, A. W. *ACS Nano* **2015**, *9*, 6188–6195, PMID: 26046586.

(11) Hopcroft, M.; Nix, W.; Kenny, T. *Microelectromechanical Systems, Journal of* **2010**, *19*, 229–238.

(12) Durig, U. *J. Appl. Phys.* **2005**, *98*, 044906.

(13) Pires, D.; Gotsmann, B.; Porro, F.; Wiesmann, D.; Duerig, U.; Knoll, A. *Langmuir* **2009**, *25*, 5141–5145.

(14) Ma, S.; Scaraggi, M.; Wang, D.; Wang, X.; Liang, Y.; Liu, W.; Dini, D.; Zhou, F. *Advanced Functional Materials* **2015**, *25*, 7366–7374.

(15) Johnson, K. L.; Kendall, K.; Roberts, A. D. *Proceedings of the Royal Society of London A: Mathematical, Physical and Engineering Sciences* **1971**, *324*, 301–313.

(16) Persson, B. *Surface Science Reports* **2006**, *61*, 201 – 227.

(17) Scaraggi, M.; Persson, B. N. J. *The Journal of Chemical Physics* **2015**, *143*.

(18) Buff, F. P.; Lovett, R. A.; Stillinger, F. H. *Phys. Rev. Lett.* **1965**, *15*, 621–623.

(19) Doerr, A.; Tolan, M.; Prange, W.; Schlomka, J.-P.; Seydel, T.; Press, W.; Smilgies, D.; Struth, B. *Phys. Rev. Lett.* **1999**, *83*, 3470–3473.